Muonic cascades in isolated low-Z atoms and molecules

K. Kirch,[1,2,*] D. Abbott,[3,†] B. Bach,[3] P. Hauser,[1] P. Indelicato,[4] F. Kottmann,[2] J. Missimer,[1] P. Patte,[4] R. T. Siegel,[3] L. M. Simons,[1] and D. Viel[3]

[1]*Paul Scherrer Institut, CH-5232 Villigen PSI, Switzerland*

[2]*Institut für Teilchenphysik, ETH-Hönggerberg, CH-8093 Zürich, Switzerland*

[3]*College of William and Mary, Williamsburg, Virginia 23185*

[4]*Laboratoire Kastler Brossel, Ecole Normale Supérieure et Université Pierre et Marie Curie, F-75252 Paris Cedex 05, France*

(Received 16 March 1998; revised manuscript received 10 November 1998)

Muonic x-ray cascades in B, C, N, O, and Ne following muonic atom formation in B_2H_6, CH_4, C_2H_6, C_4H_{10}, N_2, O_2, and Ne were investigated. The densities of the different target gases were low enough to prevent any contact of the atom or molecule on which the formation takes place with surrounding atoms or molecules during the cascade. Using semiconductor detectors, the yields of transitions in several series with energies between 1.5 keV and 300 keV were measured. Cascade calculations were performed in order to explain the observed transition yields. The cascades could be reproduced by variation of only two parameters: the number of electrons and the muon angular momentum distribution at the starting point of the calculation. The cascade of μNe formed in monoatomic neon was described best. Moreover, muonic carbon cascades were found to differ according to the sort of hydrocarbon, demonstrating the influence of the capturing molecule's structure on the muonic cascade. By varying the number of initially available electrons, the molecular effects could be described with the cascade program. [S1050-2947(99)02005-3]

PACS number(s): 36.10.Dr

I. INTRODUCTION

Muonic atoms are formed by deceleration of muons inside the target material followed by transitions from the continuum to bound states. The bound states first populated are highly excited, and it is not understood if they belong to one atom, to several atoms of the capturing molecule, or to the entire molecule. After the capture the deexcitation (i.e., the muonic cascade to the muonic atom's ground state) develops. When the muonic transition energy exceeds the electronic ionization energy the muons may deexcite via Auger emission of electrons. Because of the energy dependence of the Auger and radiative rates the Auger effect usually dominates at higher energy levels. At lower excitation levels, when transition energies become larger, the radiative transitions dominate the cascade. At some stage of the cascade the muons are bound to single atoms and can be described by hydrogenlike wave functions perturbed by electron screening. At this stage of the cascade the further deexcitation (''quantum cascade'') becomes calculable. Phenomenological models exist which explain at least the gross features of the data concerning capture (see, e.g., [1–3]) and cascades (see, e.g., [4,5]).

However, capture of negatively charged muons (and other exotic particles such as π^-, K^-, $\bar{p}$, or Σ^-) by atomic or molecular systems and the following atomic cascade are not understood in detail. It is generally agreed that atomic muon capture takes place at kinetic energies of several tens of eV via electron emission [6–8]. There is evidence that the capture populates highly excited states above principal quantum numbers of $n=\sqrt{m_\mu/m_e}$, e.g., in μFe much higher than $n=20$ [8]. The initial angular momentum distribution of the muons is usually parametrized as a modified statistical distribution $P(l)\propto(2l+1)\exp(\alpha l)$ (see, e.g., [6,7,9,10]). The probability of capture into different atoms of composite targets is known to depend on the chemical and physical structure of the target material [1,11–15]. Moreover, it has been shown that the cascades in any one element depend on the chemical bonds and the target chemistry [10,16–19].

The materials' influence on the cascades is interesting, but only understanding the cascades in isolated systems can provide the basis for investigations in complexer materials. Unfortunately nearly all published data involve two effects: capture by the single atom or molecule, and the interaction of the system with the environment during the cascade. In the case of solid state targets, strong refilling from the surroundings always provides electrons to the muonic atoms. For light atoms the muonic cascades are then completely dominated by the Auger effect down to $n\approx5$ [5,20] and observable x-ray yields become insensitive to the initial state population.

Little data on cascades in isolated atoms or molecules has yet been acquired. This is due to the difficulty of stopping exotic particles at high rates in low density gas targets, where the exotic atoms could be isolated during typical cascade times. Using the cyclotron trap [21], this problem was resolved in the spectroscopy of antiprotonic atoms formed in low pressure[1] [O(1 kPa)] gas targets [22,23].

Measurements using the same techniques in muonic atoms (μNe) were limited at the same time to several tens of

*Electronic address: Klaus.Kirch@PSI.CH

†Present address: TJNAF, Newport News, VA 23606.

[1]1 kPa=1000 Pa=10 mbar=7.5 Torr=2.45×10^{17} atoms or molecules/cm^3 ($T\approx295$ K).

kPa [24]. However, the expected charge exchange rate constants [(cross section) × (velocity)] of order 5×10^{-9} cm^3 s^{-1} (see, e.g., [25]) for the relatively low velocity of muonic atoms in gas targets and cascade times of order 10^{-10} s imply that pressures below 10 kPa are needed to isolate the system during the muonic cascade. The measurements presented below are the systematic continuation of the previous experiments in light muonic atoms, extending the gas pressures down to typically 1 kPa. Besides the interest in the cascades and processes involved at large quantum numbers, this work was triggered by the need to know the electron configuration of different muonic states for several experiments. Proposals for parity violation experiments in the light muonic atoms boron and neon are based on the metastability of the $2S$ state [26–28], which requires complete ionization of the electron shell [20,22,24]. Laser spectroscopy of the $2S$-$2P$ level splitting in the muonic Li, Be, and B atoms is based on $2S$ metastability, too [29]. Precision crystal spectroscopy of transition energies in pionic magnesium [30], pionic nitrogen, and muonic oxygen [31,32] depends on knowledge of the electron configurations of the states involved.

Thus, the aim of the present experiments is an improvement in understanding of the formation and deexcitation process of isolated low-Z muonic atoms requiring (a) as much experimental information as possible about the muonic cascades and (b) reliable cascade calculations that allow the prediction of unobserved features of the cascades, such as the electron configuration in specific states or the yields of certain transitions. The measurements were performed at low target gas pressures at which the muonic atoms are isolated from the surrounding during their cascade. Moreover, the low pressures allow the detection of low energy x rays, for which self-absorption in the target gas is not negligible. Experimentally obtained absolute yields, independent of pressure and therefore of refilling, are interpreted using an improved Akylas-Vogel [4] cascade code. Transitions with energies between 1.5 keV and 300 keV were measured in the muonic atoms B, C, N, O, and Ne after formation in low pressure gas targets of B_2H_6, CH_4, C_2H_6, C_4H_{10}, N_2, O_2, and Ne.

The paper is organized as follows: in Sec. II the experimental setup is described; in Sec. III the cascade code is introduced with discussion of the improvements; Sec. IV gives the measured absolute x-ray yields of the cascade transitions and compares them with results of the cascade code calculation. The findings and possible implications are discussed in Sec. V.

II. EXPERIMENT

The experiments were performed at the Paul Scherrer Institute's πE5 beamline, which delivered negatively charged muons at a low momentum of 31.7 MeV/c with a momentum spread of 4% full width at half maximum. The electron contamination of the beam was reduced considerably with a Wien filter. To increase the stop density of the muons in the low pressure gas targets, the cyclotron trap [21] was used. About 1.3×10^4 μ^-/s hit the scintillator at the entrance of the trap, which reduced the muon momentum to about 20 MeV/c. The muons were then forced into circular orbits due to the magnetic field of the trap, decelerated in collisions with the target gas and guided to the trap's central region. With the cyclotron trap and the low beam momentum, the fraction of muon stops per incoming muon was of the order of 10% (depending on the gas pressure) and the stop volume around 100 cm^3. The two bore holes of the trap's magnet were used to flange a Ge detector (area: 2000 mm^2, thickness: 13 mm, Be window thickness: 0.5 mm) and a Si(Li) detector (30 mm^2, 5 mm, 40 μm) to the target chamber. The Ge detector was used to investigate transitions at energies above 6 keV. At the higher energies the efficiency calibration could be done easily with radioactive sources, at the lower energies around the Ge $K\alpha$ edge the overlap in energy with the Si(Li) detector was used to cross-check the results. The efficiency of the Si(Li) detector below 6 keV was calibrated using muonic x-ray transitions with a method described in detail in [33]. During data taking the signals of the detectors were gated with signals of the muon entrance counter with a 5 μs gate. In the data analysis appropriate time cuts were set in order to select and include in the spectra the events originating from muon stops in the gas, and to suppress background events produced by muons and electrons hitting the target chamber walls. The intensities of muonic transitions were obtained by fitting transition lines and background to the spectra. As an example, Fig. 1 shows the Lyman series of muonic boron as observed in 0.27 kPa diborane gas with the Ge detector. This was the lowest pressure used in that experiment, and as a result the signal-to-background conditions are the worst ones in the present analysis. The fit with a Gaussian to the transitions as well as the linear fit to the background are included in Fig. 1. The lines from muonic copper and zinc are due to muon stops in the brass collimators inside the bore holes of the trap. The relative yields of the muonic transitions are obtained from the line intensities, taking into account the detector efficiencies and corrections for the self-absorption of low energy x rays in the target gas and solid angle effects. Because the muon stop distribution inside the trap is pressure dependent

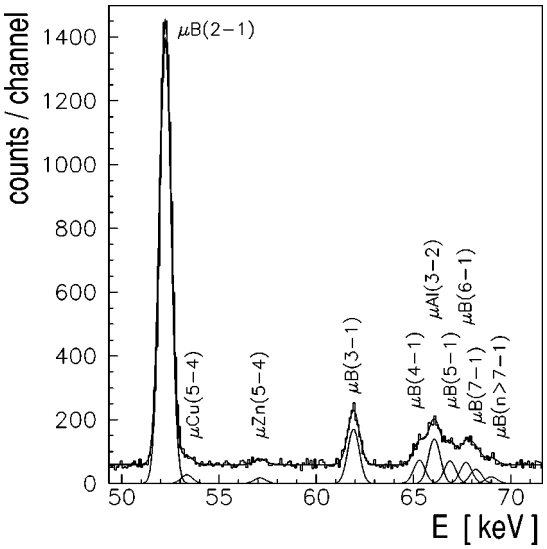

FIG. 1. Spectrum of the muonic boron Lyman series taken with the Ge detector in 0.27 kPa B_2H_6. The Gaussian fit of the transition lines and the linear background is shown. The binning is 0.096 keV per channel.

the last correction accounts for slight changes in the photon incident angles onto the detectors which lead to stronger absorption in the detector windows and inefficient layers at low energies. The probability for coincidences in one detector (e.g., the $2\rightarrow1$ and $3\rightarrow2$ transitions might simulate a $3\rightarrow1$ transition) also depends on the muon stop distribution and must be corrected for. The fact that the total yield of the muonic K series amounts to 100% (see, e.g., [34]) is used to extract absolute yields [33].

The pressure dependence of muonic cascades, in some cases down to 40 kPa, was investigated in [35]. In the experiment described here the target pressures were chosen to extend to lower pressures starting from several ten down to a fraction of a kPa. At the order of 1 kPa no pressure dependence of the observed transition yields remained (see Secs. IV and V). The small fraction of metastable $2S$ states is negligible (compare [28,33]). The relevant data leading to absolute yields given in this paper were taken at 0.27 kPa B_2H_6, 1.33 kPa CH_4, 0.67 kPa C_2H_6, 4.79 kPa C_4H_{10}, and 1.33 kPa N_2, O_2 and Ne, respectively. Such low pressures have the advantage that the absorption of the low x-ray energies inside the target gas is a small correction.

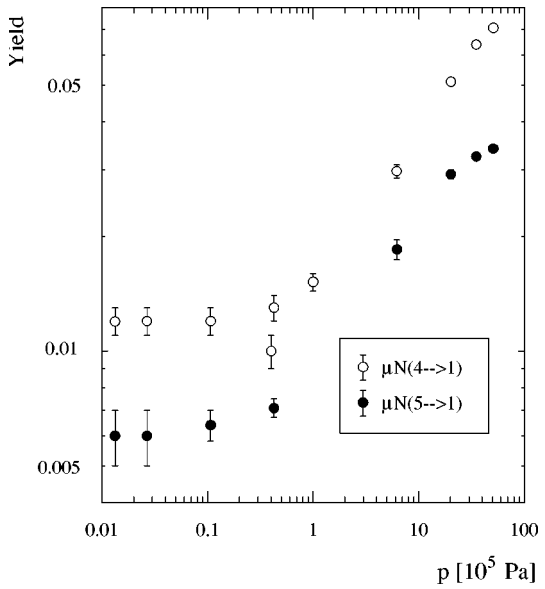

FIG. 2. Absolute yields of the muonic nitrogen Lyman transitions $4\rightarrow1$ and $5\rightarrow1$ as a function of the N_2 target gas pressure. The high pressure data are taken from [35].

III. CASCADE CODE

In the experiment atoms with $Z\leqslant10$ were investigated. Therefore the cascade calculation, based on the Akylas-Vogel code [4], described the cascade of muons in atoms with fewer than ten bound electrons, i.e., only K and L electrons. Starting with a principal quantum number n, an angular momentum distribution $P(l)$, and a specific electron configuration, the code propagates the probabilities for the different deexcitation processes (Auger monopole transitions and Auger and radiative dipole, quadrupole, and octupole transitions) and the electron configuration through all possible levels (n',l') down to the ground state. The code has been successfully applied in solids (see, e.g., [5]) and other high density materials where the muonic atom never becomes completely ionized due to electron refilling.

In order to use the code for isolated muonic systems three improvements were implemented (more details are found in the Appendix).

(1) In the original version the number of L electrons is propagated as an average value for each (n,l) state. The fact that the different transitions which populate the (n,l) state lead to a specific L electron configuration with different probabilities for $0,1,2,\ldots L$ electrons is neglected. Moreover, the L-Auger rates and transition probabilities are calculated using the product of the average numbers of electrons n_e^{av} and the $2S$- and $2P$-electron Auger rates. For $n_e^{\mathrm{av}}<1$ this leads to significant errors, because the averaging, weighted by the dominant Auger transition rates, does not take into account the cases in which no electrons are present and radiative transitions are certain. In the modified version, combined probabilities W_{n_K,n_L} of having n_K K electrons and n_L L electrons are propagated through each level (n,l).

(2) A simple model for the rearrangement of the electronic shell (internal refilling) after a K-Auger transition is included. This rearrangement is computed at each muonic state (n,l). Both radiative LK electronic transitions as well as KLL Auger effect are taken into account. The corresponding rates are taken from [36]. The refilling probability is given by the ratio $\gamma_{\mathrm{ref}}^{n_K,n_L}/(\gamma_{\mathrm{ref}}^{n_K,n_L}+\gamma_{\mathrm{depop}}^{n,l,n_K,n_L})$ where $\gamma_{\mathrm{ref}}^{n_K,n_L}$ denotes the internal refilling rate and $\gamma_{\mathrm{depop}}^{n,l,n_K,n_L}$ is the total depopulation rate (decay rate) of the (n,l) state with n_K K electrons and n_L L electrons.

(3) In the original code an average binding energy for the K electrons is used. The modified version distinguishes between the K-ionization energies for one or two K electrons. This has an important influence on the cascade of highly ionized muonic atoms between $n\approx12$ and $n\approx8$.

The cascade code deals only with atoms and therefore neglects molecular effects during the capture process and the first cascade steps. It is, however, possible to introduce more electrons into the system than can be provided by a single atom of nuclear charge Z. It is even possible to introduce more than the ten electrons that fill up the electronic K and L shells. These electrons can be considered as a reservoir provided by the molecule for refilling during the cascade.

IV. RESULTS

Figure 2 shows the pressure dependence of the $\mu N_{4\rightarrow1}$ and $\mu N_{5\rightarrow1}$ transitions. The data points at 0.04, 0.10, 0.62, 2.02, 3.52, and 5.12 MPa are taken from [35], the low pressure data taken at 42.6, 10.6, 2.7, and 1.3 kPa are from the present experiment. The investigation of the pressure dependence revealed the strongest influence on the cascades of μN and μO originating in the diatomic molecules N_2 and O_2. The prompt (i.e., not resolvable from the instant of muon stop) μC cascades from the hydrocarbon targets were found to be less pressure dependent. The μC cascades are influenced by the transfer reaction $\mu p+C\rightarrow p+\mu C$ down to low pressures. However, it is possible to resolve the transfer component of the cascade yields due to its observation in the time delayed spectra after the prompt muon stops. It was found that $W_{\mathrm{H}}^{\mu}(CH_4)=3.6(4)\%$ of the muons stopping in

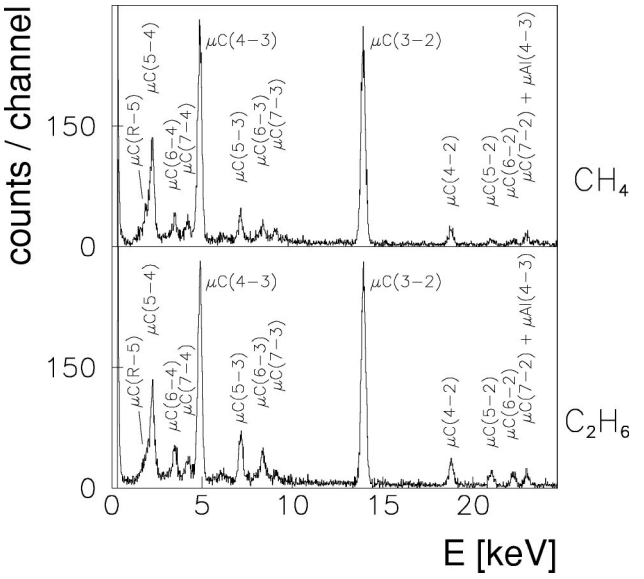

FIG. 3. Spectra of muonic carbon taken with a Si(Li) detector in CH_4 at 1.33 kPa and C_2H_6 at 0.67 kPa, respectively. The cascades reached the pressure independent regime. There is a contamination at the μC(7-2) position due to transitions μAl(4-3). The binning is 0.0215 keV per channel.

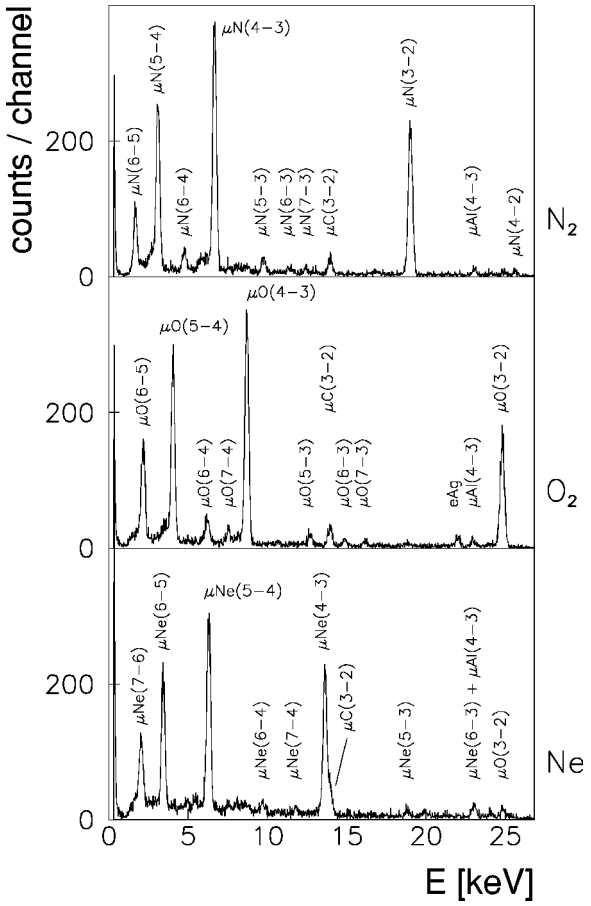

FIG. 4. Muonic x-ray spectra taken with a Si(Li) detector in N_2, O_2, and Ne at 1.33 kPa. There are contaminations due to the lines μC(3-2) and μAl(4-3). The binning is 0.0215 keV per channel.

CH_4 form μp atoms which contribute to the external transfer reaction, i.e., transfer to a molecule or an atom other than the capturing molecule. The corresponding fraction for μp formation in C_2H_6 is $W_H^{\mu}(C_2H_6)=2.9(4)\%$. The transfer rates show a linear pressure dependence and can be normalized to liquid hydrogen density (4.25×10^{22} atoms/cm^3); the resulting rates are $\lambda_T^{CH_4}=2.3(5)\times10^{10}$ s^{-1} and $\lambda_T^{C_2H_6}=5.4(10)\times10^{10}$ s^{-1}. It should be mentioned that the determination of the μp formation probabilities does not account for the fraction of μp atoms which might contribute to the transfer with much larger rates and would thus not be present in the time delayed spectra. That this fraction must be small will be discussed below in Sec. V D. In the evaluation of the μC cascade yields a correction for external transfer was applied. This is, however, a very small correction at the lowest pressures because the muon decay rate strongly exceeds the transfer rate. The absolute yield values given below are thus representing the limit of isolated molecules.

Typical experimental spectra are shown in Fig. 1 for the germanium detector and in Figs. 3 and 4 for the Si(Li) detector. The muonic copper and zinc lines in Fig. 1 are due to muon stops in brass collimators in front of the detector. The muonic carbon found in the spectra of Fig. 4 is due to muon stops in the scintillation counter and in the polyethylene cladding of the target chamber. The chamber itself is made of aluminum, and muons stopping in uncladded regions cause background lines in all spectra of Figs. 3 and 4. The spectrum of muonic oxygen in Fig. 4 contains a silver x-ray fluorescence line. This line originates in silver inside the detector and is induced by the strong μO(3-2) transition. The contribution of contamination lines to line intensities of interest was measured in another gas and was used for correction after proper normalization to the number of incoming muons. Thus, for example, the carbon contamination in the hydrocarbons was measured using the nitrogen and oxygen target. Carefully comparing the different spectra of Fig. 4 reveals more pronounced noncircular lines ($n,l\leqslant n-2\rightarrow n'\leqslant n-2,l'$) in μN and μO formed in molecules than in μNe from the atomic target. The same effect, but much more obvious, is found in Fig. 3. The muonic carbon from the C_2H_6 target shows a more noncircular cascade than the muonic carbon formed in CH_4. Since these cascades are not affected by pressure, the difference demonstrates the presence of intrinsic molecular effects, i.e., the molecule in which formation takes place influences the muonic atom cascade.

The measured absolute yields for the different x-ray series are given in Tables I, II, and III. Similarities in the data suggested grouping the results for N, O, Ne and B, C, respectively. For C_4H_{10} only data for the *K* series are available. The tables also summarize the results of the cascade calculations. These calculations of the quantum cascades were started at principal quantum number $n=16$. Initially an assumption that atomic muon capture takes place for $n\geqslant16$ was confirmed by agreement with measured yields. The distribution of initial angular momenta l is described by $P(l)\propto(2l+1)e^{\alpha l}$ with one adjustable parameter α. The number n_e of initially available electrons is not necessarily an integer, i.e., a value of 5.5 suggests that n_e is 5 in 50% of the cascades and 6 in the remaining 50%. The values for α and n_e given in the table captions lead to the least mean square deviations between measured and calculated yields.

TABLE I. Measured and calculated absolute muonic transition yields of μN, μO, and μNe from N_2 ($n_e = 4.7^{+0.3}_{-0.4}$, $\alpha = 0.040^{+0.010}_{-0.015}$), O_2 ($n_e = 6.2^{+0.3}_{-0.2}$, $\alpha = 0.065^{+0.015}_{-0.010}$), and Ne ($n_e = 4.7^{+0.8}_{-0.3}$, $\alpha = 0.090^{+0.035}_{-0.015}$), respectively. The highest and not resolved transitions of one series are grouped together in the yield $Y_{R\to\dots}$. Starting point for the calculations is the principal quantum number $n = 16$.

Absolute	N_2		O_2		Ne	
yields	Measured	Calculated	Measured	Calculated	Measured	Calculated
$Y_{7\to6}$					0.719(61)	0.702
$Y_{6\to5}$	0.621(56)	0.658	0.654(50)	0.605	0.689(44)	0.741
$Y_{7\to5}$	0.090(12)	0.065	0.080(11)	0.078	0.044(8)	0.052
$Y_{5\to4}$	0.708(35)	0.701	0.661(33)	0.649	0.775(30)	0.772
$Y_{6\to4}$	0.069(10)	0.049	0.079(9)	0.066	0.042(4)	0.044
$Y_{7\to4}$	0.038(7)	0.033	0.050(7)	0.040	0.022(6)	0.026
$Y_{4\to3}$	0.766(25)	0.760	0.740(25)	0.717	0.820(30)	0.818
$Y_{5\to3}$	0.044(8)	0.042	0.044(7)	0.052	0.031(7)	0.035
$Y_{6\to3}$	0.019(6)	0.020	0.024(7)	0.029	0.019(5)	0.018
$Y_{7\to3}$	0.020(6)	0.023	0.024(7)	0.028	0.011(3)	0.017
$Y_{8\to3}$	0.009(4)	0.014	0.008(5)	0.006	0.003(2)	0.004
$Y_{3\to2}$	0.834(9)	0.832	0.801(24)	0.802	0.872(13)	0.875
$Y_{4\to2}$	0.037(1)	0.037	0.029(21)	0.044	0.028(5)	0.030
$Y_{5\to2}$	0.012(1)	0.012	0.017(2)	0.016	0.010(4)	0.010
$Y_{6\to2}$	0.003(2)	0.011	0.012(3)	0.019	0.011(4)	0.011
$Y_{7\to2}$			0.017(2)	0.022	0.010(4)	0.013
$Y_{8\to2}$			0.009(3)	0.006	0.005(2)	0.004
$Y_{R\to2}$	0.039(3)	0.031	0.003(3)	0.000		
$Y_{2\to1}$	0.927(8)	0.925	0.888(10)	0.911	0.938(4)	0.945
$Y_{3\to1}$	0.027(7)	0.029	0.040(7)	0.034	0.024(3)	0.022
$Y_{4\to1}$	0.012(1)	0.009	0.022(3)	0.011	0.007(2)	0.006
$Y_{5\to1}$	0.006(1)	0.005	0.011(2)	0.008	0.008(1)	0.004
$Y_{6\to1}$			0.014(3)	0.013	0.009(1)	0.007
$Y_{7\to1}$			0.019(3)	0.017	0.009(1)	0.009
$Y_{R\to1}$	0.029(2)	0.032	0.006(3)	0.006	0.005(1)	0.005

V. DISCUSSION

The comparison of experimental and theoretical yields in Tables I, II, and III is based on calculations starting at principal quantum number $n = 16$. This specific n value was chosen in order to treat the seven muonic atoms on the same footing. It is important to keep in mind that starting the calculation at a particular n value implies only that muonic atom formation takes place for n' with $n' \geq n$.

A. Pressure independence of the yields

The aim of the experiment was to measure muonic x-ray yields in isolated atoms and molecules. Therefore the measurements had to be performed in a pressure region at which the cascade yields were no longer pressure dependent. The measurements of the present experiment were performed in that region. The two muonic nitrogen transitions $\mu N_{4\to1}$ and $\mu N_{5\to1}$ of Fig. 2 are best suited to demonstrate the constancy of the yields at low pressures. There are technical reasons as well as physical motivations for this choice. The technical reasons are the following: the measurable transition intensities are nearly independent of the muon stop distribution; they are insensitive to self-absorption in the target because of their relatively high energy (larger 120 keV); the transition energy cannot be produced in a coincidence of two circular transitions because the transitions have $\Delta n > 2$; and, finally, these transitions are—depending on the state of the electron shell—in competition with dipole $\Delta n = 1$ Auger transitions and because of their low yields they can therefore show large relative effects.

The physics motivation to look at the nitrogen transitions arises because the cascade of μN formed in the diatomic nitrogen molecules has already proven to be much more dependent on the target gas pressure than the cascade of neon originating in an atomic target [35]. This difference in pressure dependence has been explained in terms of a Coulomb explosion of the nitrogen molecule following the ejection of several electrons.

In the carbon cascade in CH_4 only H ions might accelerate the μC system. This explains the result of the present investigation that the μC cascade is less pressure dependent than the one of μN. The fact that the carbon cascade in C_2H_6 was also found to be less pressure dependent than the μN cascade indicates that the Coulomb explosion of that molecule could be buffered due to the additional hydrogen atoms. As already stressed above, the statements about pressure independence are valid only for the prompt cascade (these values are contained in Table II), not for the μC cascade following a transfer reaction after muon capture on hydrogen (see below).

TABLE II. Measured and calculated absolute muonic transition yields of μB and μC from B_2H_6 ($n_e=8.4\pm0.2$, $\alpha=-0.06\pm0.01$), CH_4 ($n_e=5.7\pm0.1$, $\alpha=-0.065\pm0.005$), and C_2H_6 ($n_e=7.8\pm0.1$, $\alpha=-0.080\pm0.005$). The highest and not resolved transitions of one series are grouped together in the yield $Y_{R\to\ldots}$. Starting point for the calculations is the principal quantum number $n=16$.

Absolute	B_2H_6		CH_4		C_2H_6	
yields	Measured	Calculated	Measured	Calculated	Measured	Calculated
$Y_{5\to4}$	0.50(30)	0.44	0.501(11)	0.494	0.386(11)	0.391
$Y_{6\to4}$	0.11(4)	0.09	0.070(5)	0.069	0.087(5)	0.097
$Y_{7\to4}$		0.02	0.051(5)	0.048	0.052(4)	0.029
$Y_{4\to3}$	0.490(40)	0.502	0.571(7)	0.570	0.454(8)	0.456
$Y_{5\to3}$	0.080(20)	0.077	0.066(3)	0.060	0.094(4)	0.078
$Y_{6\to3}$			0.042(2)	0.036	0.062(2)	0.066
$Y_{7\to3}$			0.033(2)	0.038	0.024(2)	0.023
$Y_{8\to3}$			0.014(2)	0.018	0.004(2)	0.002
$Y_{R\to3}$	0.120(30)	0.078				
$Y_{3\to2}$	0.621(19)	0.607	0.665(8)	0.678	0.556(8)	0.570
$Y_{4\to2}$	0.062(11)	0.063	0.065(2)	0.056	0.085(2)	0.066
$Y_{5\to2}$	0.037(8)	0.049	0.029(2)	0.023	0.051(2)	0.048
$Y_{6\to2}$			0.026(2)	0.028	0.044(2)	0.062
$Y_{7\to2}$			0.024(5)	0.035	0.022(6)	0.023
$Y_{8\to2}$			0.024(2)	0.018	0.010(2)	0.025
$Y_{R\to2}$	0.063(13)	0.073	0.009(2)	0.002	0.002(2)	0.000
$Y_{2\to1}$	0.783(9)	0.798	0.842(3)	0.842	0.770(4)	0.776
$Y_{3\to1}$	0.073(5)	0.063	0.061(2)	0.052	0.082(2)	0.068
$Y_{4\to1}$	0.040(3)	0.031	0.020(2)	0.019	0.040(2)	0.032
$Y_{5\to1}$	0.036(4)	0.040	0.012(1)	0.014	0.032(2)	0.040
$Y_{6\to1}$	0.036(4)	0.049				
$Y_{7\to1}$	0.022(4)	0.018				
$Y_{R\to1}$	0.011(4)	0.001	0.065(2)	0.072	0.076(2)	0.083

B. Muonic neon

The best agreement between calculation and the experimental yields is obtained for μNe. This is not very surprising because atomic neon is the simplest of the targets used and the one for which the atomic cascade code is best suited. Figure 5 shows the 1σ ($\chi^2=\chi^2_{\min}+1$) and 2σ ($\chi^2=\chi^2_{\min}+4$) contours of the sum of the squared deviations

$$\chi^2=\sum_{n,n'}(Y^{\text{calc}}_{n\to n'}-Y^{\text{expt}}_{n\to n'})^2/(\Delta Y^{\text{expt}}_{n\to n'})^2$$

between calculated and measured yields in the plane of α versus n_e. The correlation of the two parameters is obvious. The χ^2 value reaches a minimum of $\chi^2_{\min}\approx13$ for the 24 transitions, indicating overestimation of systematic experimental errors. The main systematic error is caused by the unknown shape of the background in the spectra from which transition line intensities are extracted. The error values given in this paper are always conservatively estimated and thus might yield the low $\chi^2_{\min}$. Consequently, the errors given for α and n_e might be slightly overestimated.

TABLE III. Measured and calculated absolute K yields of μC from C_4H_{10} ($n=16$, $\alpha=0.0$, $n_e=13.5\pm1.0$).

Absolute	C_4H_{10}	
yields	Measured	Calculated
$Y_{2\to1}$	0.689(20)	0.695
$Y_{3\to1}$	0.129(13)	0.109
$Y_{4\to1}$	0.109(10)	0.126
$Y_{5\to1}$	0.055(9)	0.057
$Y_{R\to1}$	0.018(7)	0.013

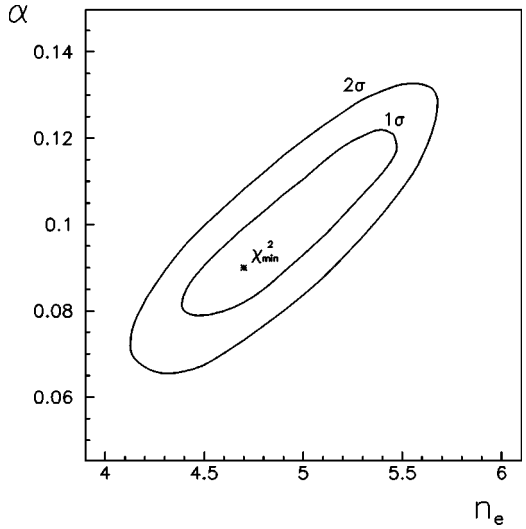

FIG. 5. χ^2 contour plot in the α-n_e plane for μNe. The starting point of the calculation is at $n=16$. One extracts $n_e=4.7^{+0.8}_{-0.3}$ and $\alpha=0.090^{+0.035}_{-0.015}$.

TABLE IV. Total level energies for muonic neon at muonic principal quantum number n_μ. The total level energy is defined as the difference between the mass of the atom in a specific state and the masses of the constituents (nucleus, muon, electrons). The energy values are given in eV.

n_μ	Electron core	Level energy	n_μ	Electron core	Level energy
12	He $1s^2$	−4076.2	16	N $1s^2\,2s^2\,2p^3$	−3921.9
13	He $1s^2$	−3808.9	17	N $1s^2\,2s^2\,2p^3$	−3822.5
14	He $1s^2$	−3602.7	18	N $1s^2\,2s^2\,2p^3$	−3742.9
15	He $1s^2$	−3442.1	19	N $1s^2\,2s^2\,2p^3$	−3678.4
			20	N $1s^2\,2s^2\,2p^3$	−3625.5
12	Li $1s^2\,2s$	−4264.5	21	N $1s^2\,2s^2\,2p^3$	−3581.6
13	Li $1s^2\,2s$	−3998.0	22	N $1s^2\,2s^2\,2p^3$	−3544.9
14	Li $1s^2\,2s$	−3792.7	23	N $1s^2\,2s^2\,2p^3$	−3513.9
15	Li $1s^2\,2s$	−3632.9			
16	Li $1s^2\,2s$	−3507.2	17	O $1s^2\,2s^2\,2p^4$	−3859.1
			18	O $1s^2\,2s^2\,2p^4$	−3779.3
12	Be $1s^2\,2s^2$	−4421.2	19	O $1s^2\,2s^2\,2p^4$	−3714.7
13	Be $1s^2\,2s^2$	−4155.3	20	O $1s^2\,2s^2\,2p^4$	−3661.7
14	Be $1s^2\,2s^2$	−3950.8	21	O $1s^2\,2s^2\,2p^4$	−3618.0
15	Be $1s^2\,2s^2$	−3791.7	22	O $1s^2\,2s^2\,2p^4$	−3581.6
16	Be $1s^2\,2s^2$	−3666.7	23	O $1s^2\,2s^2\,2p^4$	−3551.0
17	Be $1s^2\,2s^2$	−3567.6	24	O $1s^2\,2s^2\,2p^4$	−3525.2
			25	O $1s^2\,2s^2\,2p^4$	−3503.5
14	B $1s^2\,2s^2\,2p$	−4063.5	26	O $1s^2\,2s^2\,2p^4$	−3485.4
15	B $1s^2\,2s^2\,2p$	−3904.2			
16	B $1s^2\,2s^2\,2p$	−3779.0	18	F $1s^2\,2s^2\,2p^5$	−3795.5
17	B $1s^2\,2s^2\,2p$	−3679.6	19	F $1s^2\,2s^2\,2p^5$	−3731.1
18	B $1s^2\,2s^2\,2p$	−3599.9	20	F $1s^2\,2s^2\,2p^5$	−3678.3
19	B $1s^2\,2s^2\,2p$	−3535.2	21	F $1s^2\,2s^2\,2p^5$	−3634.6
			22	F $1s^2\,2s^2\,2p^5$	−3598.1
15	C $1s^2\,2s^2\,2p^2$	−3990.8	23	F $1s^2\,2s^2\,2p^5$	−3567.4
16	C $1s^2\,2s^2\,2p^2$	−3865.7	24	F $1s^2\,2s^2\,2p^5$	−3541.6
17	C $1s^2\,2s^2\,2p^2$	−3766.5	25	F $1s^2\,2s^2\,2p^5$	−3519.8
18	C $1s^2\,2s^2\,2p^2$	−3687.1	26	F $1s^2\,2s^2\,2p^5$	−3501.7
19	C $1s^2\,2s^2\,2p^2$	−3622.7	27	F $1s^2\,2s^2\,2p^5$	−3487.0
20	C $1s^2\,2s^2\,2p^2$	−3569.9	28	F $1s^2\,2s^2\,2p^5$	−3484.9
21	C $1s^2\,2s^2\,2p^2$	−3526.0			

Since muonic neon binds nine electrons immediately after muon capture and, on the average four or five electrons at the starting point of the cascade calculation ($n=16$), the atom must have undergone four to five Auger deexcitations to reach $n\approx 16$, implying its formation at a principal quantum number $n\geqslant 20$. This consideration offers the possibility to determine the levels at which muon capture in neon atoms takes place. Checking the probabilities of Auger transitions requires exact knowledge of the total binding energies of the system, which consists of the neon nucleus, the muon in different states, and electrons in different configurations.

To calculate the binding energies we used the latest version of Desclaux's multiconfiguration Dirac-Fock code [37–39], which has been generalized by Indelicato to accommodate exotic atoms with arbitrary electronic structure. In contrast to older codes, this program can account for full recoupling between the electrons and the exotic particles. The code is fully relativistic, and includes Breit and higher order retardation corrections. The magnetic interaction is treated self-consistently on the same footing as the Coulomb interaction [40]. In order to get accurate energy, radiative corrections for electrons (self-energy, self-energy screening, and vacuum polarization [37,38]) and the muon (vacuum polarization) are included. More details will be published elsewhere.

Calculated total level energies are given in Table IV. One result of the calculation which was not expected in advance (compare, e.g., [41]) was that the muonic fine structure splitting within principal quantum numbers n_μ under consideration is below 0.1 eV. As another important result the dominance of the $\Delta n=1$ Auger transitions below $n=16$ is proven. This corroborates the possibility of treating L electrons in a relatively rough fashion in the cascade code, whereas the K-electron situation is accounted for in more detail. Figure 6 shows the possible Auger cascade chains leading to the required electron configuration at $n=16$. There are several $\Delta n=2$ Auger steps required for which quadrupole transitions for maximum l states are necessary. At the low transition energies involved at those high n levels the quadrupole transitions still dominate the possible radiative dipole transitions completely (see, e.g., [5]). The limiting cascades (full black circles and rectangles) give four and

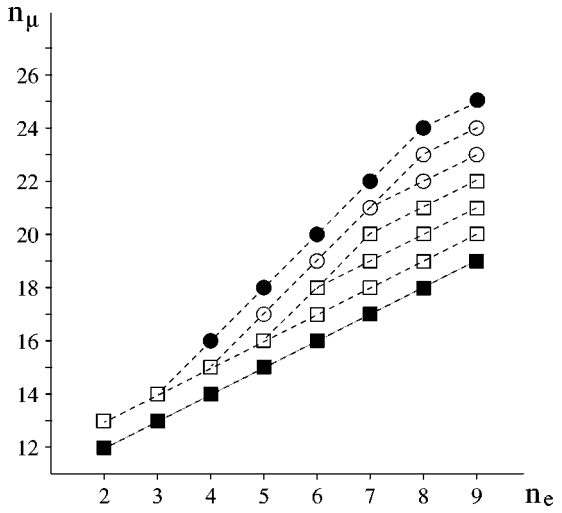

FIG. 6. Auger decay chains allowed by the total binding energies of Table IV and covering the possible electron configurations at principal quantum number $n_\mu = 16$ (compare Fig. 5).

six electrons at $n = 16$, both of which are quite improbable, as shown in Fig. 5. Therefore it is concluded that the muon capture takes place at principal quantum numbers between 20 and 24.

C. Diatomic molecules

Concerning the muonic atoms μN and μO, comparison with μNe reveals stronger noncircular yields for the muonic atoms formed on the molecular targets. The correlation of α and n_e for μN and μO is qualitatively the same as for μNe (see Fig. 5). Both α_N and α_O are smaller than α_{Ne}. Thus describing the three cascades by one mean α value requires one electron more for μN and two more for μO than for μNe. We assume that the levels into which the muons are captured have similar binding energies, implying that it would take a similar number of muonic transitions to reach the state with $n = 16$ where our calculation starts. Ten to eleven electrons appear to be involved in μN and μO in molecular N_2 and O_2, respectively, while only six or seven electrons can be provided by an isolated constituent atom. This is consistent with the pressure dependence observed in the μN cascade in N_2 compared to that in μNe in Ne [35]: similar cascades were found in both cases but at lower pressures in N_2 than in Ne. This observation has been explained in terms of a Coulomb explosion, in which the molecular fragments (μN^{i+}, N^{j+}) produced in the first steps of the cascade gain high kinetic energies due to repulsion. This leads to increased collision rates with electron refilling and consequently to more pressure dependent cascades in μN than in μNe. Assuming symmetric ionization $i \approx j$, we estimate $i \approx 3-4$ and, moreover, kinetic energies of the molecular fragments of the order of several tens of eV.

D. Hydrocarbons: hydrogen capture probability and transfer

It has already been mentioned that the determination of the muon capture probabilities W_H^μ relies on the observation of time delayed transfer and therefore does not take into account a very fast transfer component. Because the μp atoms will very probably leave the molecule on which formation took place only in states with low principal quantum numbers ($n \approx 5-6$) [1] the remaining cascade is too fast to allow for excited state transfer. A fast component can only be due to the transfer from μp atoms in $2S$ states. The $2S$ population in muonic hydrogen is known only for μp formation in hydrogen targets [42] and it is below 7% for pressures at which collisional effects do not influence the μp cascade at $n \leqslant 5$. Adopting this result to the present problem leads to an upper limit of 7% for a fast transfer component. The experimental errors of 11% and 14% for $W_H^\mu(CH_4)$ and $W_H^\mu(C_2H_6)$, respectively, take into account this conceivable fast component. Additional confirmation that only a small fraction of μp belongs to a fast transfer component comes from comparison with πp data. In the πp case the $2S$ states will not contribute to the transfer.

The published measurements of negative pion capture probabilities on hydrogen in CH_4 and C_2H_6 targets are $W_H^\pi(CH_4) = 2.473(53)\%$ [43] and $W_H^\pi(C_2H_6) = 1.877(53)\%$ [44]. No dependence on the target density had been found for the formation probability of πp on C_2H_6, even over a region covering two orders of magnitude [45]. The fact that the probabilities for muon capture from the present experiment are larger is due to the much lower target gas pressures, and not to any difference between pions and muons. With the most refined version of the model of large mesic molecules [3,19] the pion data can be explained. This version of the model does not contain an explicit pressure dependent parameter. However, it contains a parameter which describes the ''nontransfer probability;'' this probability should be 1 at the lowest pressures. Assuming this value and accepting the other parameters of [3] one finds $W_H^\pi(CH_4) = 3.5\%$ and $W_H^\pi(C_2H_6) = 3.0\%$ as the ''isolated molecule limit.'' These values are in a good agreement with our results.

Concerning the transfer rates, the larger value for C_2H_6 than for CH_4 probably reflects only that the number of carbon atoms is twice as large in C_2H_6. For the small, neutral μp system the carbon atoms are nearly isolated even in the C_2H_6 molecule (compare [12]). The transfer rate in CH_4 can be compared with another measurement which found a value of $9.5(5) \times 10^{10}$ s^{-1} in a mixture of $H_2 + 0.17\%$ CH_4 at pressures between 1 and 4 MPa [46]. At such high pressures most of the μp are thermalized at the instant of ground state transfer. The lower transfer rate found in the present experiment can be attributed to a decreasing transfer cross section with increasing μp kinetic energy. The μp formed on the hydrocarbon might be accelerated during the cascade, due to deexcitation in the Coulomb field of hydrogen and carbon atoms similar to the Coulomb deexcitation of μp formed in H_2. Because of the low gas pressures, the μp do not undergo enough elastic collisions to thermalize during the muon lifetime. A recent experiment with low pressure gas targets [$O(100\,\text{Pa})$] found similar kinetic energy distributions of μp in CH_4 and H_2, respectively [47].

E. Hydrogen compounds: cascades

Despite the differences observed in μN, μO, and μNe, there are similarities such as the positive values of α, which shift the muonic l distribution towards large values. The μB and μC cascades originating in hydrogen compounds are

quite different. Their cascades are reproduced with negative values of α which shift the muonic l distribution towards lower l values. [In the case of C_4H_{10}, where the cascade has been reproduced with a purely statistical distribution ($\alpha = 0$), there is less sensitivity to the exact value of α.] The shift in the l distribution can be explained by a simple argument: the angular momenta of the states into which the muons are captured depend on the muons' kinetic energy and the impact parameter relative to the capturing atom. As the formation process usually takes place on valence electrons, the impact parameter is correlated with the distribution of these electrons in the system. In the case of the C—H or B—H bonds of the hydrogen compounds, the electrons are usually located between the atoms and the impact parameter is limited by the bond length. In the case of the monatomic or diatomic gases there is no such limitation. In fact, the orbital radius of the outer Ne electrons exceeds the C—H bond length by 40%. Assuming similar kinetic energies for capture on the different atoms and molecules (compare [2,48]) then indicates higher angular momenta for muon capture by N_2, O_2, and Ne. As the initial muonic cascades proceed via Auger effect, which only slightly influences the shape of the l distribution (see [6]), the shift in the l distribution is preserved down to quantum numbers around $n = 16$.

Concerning the cascades in μC from different hydrocarbons the trend is clear: smaller molecules produce more circular cascades. In terms of the model this corresponds to fewer molecular electrons leading to more circular cascades. Since it was shown that the cascade begins above $n = 16$, comparison with the calculation suggests that the molecules are still not completely fragmented when the muons reach orbits at $n = 16$. An isolated carbon atom would provide at most five electrons after atomic muon capture proceeding via electron ejection. However, there is no way within the present cascade model to reproduce the measured yields without increasing the number of electrons. In the case of C_4H_{10}, the situation is extreme because even more electrons than the L shell could hold must be introduced. This supports the assumption that the muonic cascade proceeds inside the molecule until the molecule is destroyed by the repulsion of positively charged Coulomb centers at relatively low n values.

An interesting point concerning the cascade of μB in B_2H_6 should be mentioned: The measured μB yields are always between the μC yields in CH_4 and C_2H_6 but the values of the input parameters of the cascade calculation for B_2H_6 are close to those for C_2H_6, in fact they can be reproduced with the same α and n_e. This means that the differences in measured yields in B_2H_6 and C_2H_6 originate mainly from the different nuclear charges of boron and carbon. Since the molecular structures of B_2H_6 and C_2H_6 are completely different, this finding corroborates the interpretation that the molecules provide electrons as a reservoir for the muonic cascade while molecular structure has little influence.

VI. CONCLUSIONS

Sets of muonic x-ray transitions in low-Z atoms have been measured in gases at low pressures with the cyclotron trap. The gas pressures were sufficiently low that the cascades were not influenced by collisions with the surrounding atoms and molecules. Moreover, measurements of low energy x rays emitted in transitions between relatively high excited levels could be made. The following conclusions are drawn from the measurements.

(i) The measured muonic cascades are pressure independent below target gas pressures of a few kPa.

(ii) The reproduction of the measured x-ray yields is possible using an atomic cascade calculation starting at principal quantum number $n = 16$. The differences in the cascades of the various gases can be described by varying the initial angular momentum distribution of the muons and the number of initially available electrons to simulate molecular effects.

(iii) Most of the capture of muons by neon atoms takes place at muonic principal quantum numbers between 20 and 24 and dominantly at high angular momenta. The measurements described might permit the calculation of the kinetic energy distribution of the muons before capture by neon.

(iv) The measurements clearly demonstrate that the muonic cascades depend on the capturing molecule, not only on the constituent, participating atom. This is evident in the measurements of μC cascades in different hydrocarbons.

(v) The capture of muons by atoms and molecules depends on the structure of the target atom or molecule itself. Two groups of angular momentum distributions were found: distributions dominated by higher angular momentum (compared to the statistical distribution) observed in monatomic or diatomic targets, and distributions dominated by lower angular momentum observed in hydrogen compounds. This can be understood classically in terms of the limited impact parameters in hydrogen compounds.

(vi) Since the cascade calculations are started at $n = 16$ and more electrons than one atom could provide are usually present, it is evident that the molecules are not fully fragmented at this stage of the cascade. Whether the muon is in a molecular orbit or the molecule serves only as electron reservoir for internal refilling to the muonic atom cannot yet be determined.

(vii) With improved understanding of the muonic cascades in isolated systems, it becomes possible to study the pressure dependence. Various spectroscopic methods might be applied to extract the kinetic energies of highly ionized muonic atoms (typically expected in the eV range) and electron refilling cross sections in collisions with surrounding atoms and molecules which will be relevant to conventional ions with nuclear charge $Z-1$.

ACKNOWLEDGMENTS

It is a pleasure to thank B. Leoni for his great technical support, the PSI staff for providing us with excellent conditions for our experiments, and R. Pohl, S. Romanov, and D. Taqqu for fruitful discussions.

APPENDIX: MODIFICATION OF AKYLAS-VOGEL CODE

1. Propagation of the electron configuration through the cascade

In the modified Akylas-Vogel code the electron configurations of K and L electrons are propagated through each

muonic level (n,l) as a set of 27 different probabilities $P_{n_K,n_L}(n,l)$ of having $n_K=0,1,2$ K electrons together with $n_L=0,1,\ldots,8$ L electrons. We start with a state with main quantum number n_1 and angular momentum l_1 and define $C(n_1,l_1)$ as the probability that the cascade goes through this level. The contribution $\varepsilon_{n_K,n_L}(n_1,l_1;n_2,l_2)$ to the electron configuration $P_{n_K,n_L}(n_2,l_2)$ of a level n_2,l_2 $(n_2 \leqslant n_1)$ due to a specific $(n_1,l_1 \rightarrow n_2,l_2)$ transition is then

$$\varepsilon^{\mathrm{rad}}_{n_K,n_L}(n_1,l_1;n_2,l_2) = \Gamma^{\mathrm{rad}}/\Gamma^{\mathrm{tot}}_{n_K,n_L}(n_1,l_1)P_{n_K,n_L}(n_1,l_1)C(n_1,l_1),$$

$$\varepsilon^{A_K}_{n_K,n_L}(n_1,l_1;n_2,l_2) = \Gamma^{A_K}_{n_K+1}/\Gamma^{\mathrm{tot}}_{n_K+1,n_L}(n_1,l_1)P_{n_K+1,n_L}(n_1,l_1) \times C(n_1,l_1), \qquad n_K=0,1 \tag{A1}$$

$$\varepsilon^{A_L}_{n_K,n_L}(n_1,l_1;n_2,l_2) = \Gamma^{A_L}_{n_L+1}/\Gamma^{\mathrm{tot}}_{n_K,n_L+1}(n_1,l_1)P_{n_K,n_L+1}C(n_1,l_1), \quad n_L \leqslant 7.$$

$\Gamma^{\mathrm{tot}}_{n_K,n_L}(n_1,l_1)$ is the total depopulation rate (transition rate) of the level (n_1,l_1), Γ^{rad} is the radiative transition rate, $\Gamma^{A_K}_{n_K'}$ is the K-Auger transition rate with n_K' K electrons, and $\Gamma^{A_L}_{n_L'}$ is the L-Auger transition rate with n_L' L electrons. The Auger rates are computed according to the original Akylas-Vogel code. The K-Auger rates are proportional to the number of K electrons present. In the case of L-Auger transitions the $2S$ and $2P$ electron configurations are not propagated separately. As in the original code, the L-Auger transition rates are calculated for fixed relative contributions P_{2S} of $2S$ electrons and P_{2P} of $2P$ electrons $(P_{2S}+P_{2P}=1)$ during the whole cascade. P_{2S} and P_{2P} are given by the input values $N^i_{2S}=n^i_L P_{2S}$ and $N^i_{2P}=n^i_L P_{2P}$ at the beginning of the cascade, where n^i_L is the total number of L electrons at the starting point.

From Eq. (A1) follows for the electron configuration $P_{n_K,n_L}(n_2,l_2)$ and the probability $C(n_2,l_2)$ that the cascade goes through n_2,l_2 the relation

$$C(n_2,l_2)P_{n_K',n_L'}(n_2,l_2) = \sum_{n_1,l_1} [\varepsilon^{\mathrm{rad}}_{n_K',n_L'}(n_1,l_1;n_2,l_2) + \varepsilon^{A_K}_{n_K',n_L'}(n_1,l_1;n_2,l_2) + \varepsilon^{A_L}_{n_K',n_L'}(n_1,l_1;n_2,l_2)], \tag{A2}$$

where the sum goes over all levels with $n_1 > n_2$ $(n_1=n_2$ is only considered for $n_1=2)$ and $-3 \leqslant (l_1-l_2) \leqslant 3$. The normalization of $P_{n_K,n_L}(n_2,l_2)$,

$$\sum_{n_K'=0}^{2}\sum_{n_L'=0}^{8} P_{n_K',n_L'}(n_2,l_2)=1, \tag{A3}$$

then leads to the determination of $C(n_2,l_2)$.

2. Implementation of two different ionization energies of K electrons

The original cascade code did not distinguish between the ionization of an atom with two K electrons remaining and of one with only one remaining K electron. The average K-ionization energy is replaced as input parameter by two individual ionization energies which are usually given by the corresponding binding energies of a $Z-1$ atom where Z is the atomic number. This modification affects the calculated K-Auger probabilities at intermediate $n=8,\ldots,12$ where the transition energies of $\Delta n=2$ and $\Delta n=1$ transitions are close to the K-ionization energy and thus allow or inhibit the corresponding Auger transition.

3. Refilling of the K-electron shell

A simple refilling model is introduced into the cascade code which distinguishes between external and internal (radiative or Auger) refilling. The internal refilling is implemented only for K and L electrons and is therefore applicable to atoms with $Z \leqslant 10$. At low densities external refilling can be neglected and only internal refilling of a K hole with an L electron has to be considered. Two processes can lead to an electron transition from an L shell to a K shell: Radiative refilling $\Gamma^{\mathrm{ref}}_{LK}$ where an x ray is emitted, and Auger refilling $\Gamma^{\mathrm{ref}}_{KLL}$ where a second electron from the L shell is emitted. The refilling rates $\Gamma^{\mathrm{ref}}_{LK}$ and $\Gamma^{\mathrm{ref}}_{KLL}$ are introduced as two parameters which describe an atom with a complete L shell $(n_L=Z-2)$ and a single K hole (see [36]). The refilling rates with n_L' L-shell electrons and $n_K=0,1,2$ K electrons are taken as

$$\Gamma^{\mathrm{ref},LK}_{n_K,n_L'} = \Gamma^{\mathrm{ref}}_{LK}(2-n_K)n_L'/(Z-2), \quad n_L' \geqslant 1$$
$$\Gamma^{\mathrm{ref},KLL}_{n_K,n_L'} = \Gamma^{\mathrm{ref}}_{KLL}(2-n_K)n_L'/(Z-2), \quad n_L' \geqslant 2. \tag{A4}$$

In order to simplify the calculation the refilling of an intermediate state is considered before the next cascade step occurs. The refilling probability P^{ref} corresponds to the ratio of refilling rate and total depopulation rate (including Γ^{ref}) of the considered state n_2,l_2. Thus for Auger refilling $(n_K \leqslant 1, n_L' \geqslant 2)$ we get

$$P^{\mathrm{ref},KLL}_{n_K,n_L'} = \Gamma^{\mathrm{ref},KLL}_{n_K,n_L'}/[\Gamma^{\mathrm{tot}}_{n_K,n_L'}(n_2,l_2) + \Gamma^{\mathrm{ref},KLL}_{n_K,n_L'} + \Gamma^{\mathrm{ref},LK}_{n_K,n_L'}(+\Gamma^{\mathrm{ref,ext}})] \tag{A5}$$

and the corresponding rearrangement of the electron configuration is then

$$P_{n_K,n_L'}(n_2,l_2) = P_{n_K,n_L'}(n_2,l_2)(1-P^{\mathrm{ref},KLL}_{n_K,n_L'}),$$
$$P_{n_K+1,n_L'-2}(n_2,l_2) = P_{n_K,n_L'}(n_2,l_2)(1+P^{\mathrm{ref},KLL}_{n_K,n_L'}). \tag{A6}$$

[1] L. I. Ponomarev, Annu. Rev. Nucl. Sci. **23**, 395 (1973).
[2] T. von Egidy, D. H. Jakubassa-Amundsen, and F. J. Hartmann, Phys. Rev. A **29**, 455 (1984).
[3] A. Shinohara, T. Muroyama, C. Murata, T. Miura, T. Saito, A. Yokoyama, S. Kojima, and M. Furukawa, Phys. Rev. Lett. **76**, 2460 (1996).
[4] V. R. Akylas and P. Vogel, Comput. Phys. Commun. **15**, 291 (1978).
[5] P. Vogel, Phys. Rev. A **22**, 1600 (1980).
[6] F. J. Hartmann, in *Electromagnetic Cascade and Chemistry of Exotic Atoms*, edited by L. M. Simons, D. Horváth, and G. Torelli (Plenum Press, New York, 1990).
[7] K. Kaeser, T. Dubler, B. Robert-Tissot, L. A. Schaller, L. Schellenberg, and H. Schneuwly, Helv. Phys. Acta **52**, 238 (1979).
[8] F. J. Hartmann, R. Bergmann, H. Daniel, H.-J. Pfeiffer, T. von Egidy, and W. Wilhelm, Z. Phys. A **305**, 189 (1982).
[9] F. J. Hartmann, T. von Egidy, R. Bergmann, M. Kleber, H.-J. Pfeiffer, K. Springer, and H. Daniel, Phys. Rev. Lett. **37**, 331 (1976).
[10] D. Kessler, H. L. Anderson, M. S. Dixit, H. J. Evans, R. J. McKee, C. K. Hargrove, R. D. Barton, E. P. Hincks, and J. D. McAndrew, Phys. Rev. Lett. **18**, 1179 (1967).
[11] E. Fermi and E. Teller, Phys. Rev. **72**, 399 (1947).
[12] V. I. Petrukhin and V. M. Suvorov, Zh. Éksp. Teor. Fiz. **70**, 1145 (1976) [Sov. Phys. JETP **43**, 595 (1976)].
[13] H. Schneuwly, V. I. Pokrovsky, and L. I. Ponomarev, Nucl. Phys. A **312**, 419 (1978).
[14] D. Horváth, Radiochim. Acta **28**, 241 (1981).
[15] N. Imanishi, S. Miyamoto, Y. Takeuchi, A. Shinohara, H. Kaji, and Y. Yoshimura, Phys. Rev. A **37**, 43 (1988).
[16] H. Daniel, H. Koch, G. Poelz, H. Schmitt, L. Tauscher, G. Backenstoss, and S. Charalambus, Phys. Lett. **26B**, 281 (1968).
[17] A. D. Konin, V. N. Pokrovsky, L. I. Ponomarev, H. Schneuwly, V. G. Zinov, and I. A. Yutlandov, Phys. Lett. **50A**, 57 (1974).
[18] H. Daniel, F. J. Hartmann, R. A. Naumann, and J. J. Reidy, Phys. Rev. Lett. **56**, 448 (1986).
[19] A. Shinohara, T. Muroyama, J. Shintai, J. Kurachi, M. Furukawa, T. Miura, Y. Yoshimura, T. Saito, T. Ohdaira, and N. Imanishi, Phys. Rev. A **53**, 130 (1996).
[20] R. Bacher, D. Gotta, L. M. Simons, J. Missimer, and N. C. Mukhopadhyay, Phys. Rev. Lett. **54**, 2087 (1985).
[21] L. M. Simons, Phys. Scr. **T22**, 90 (1988).
[22] R. Bacher, P. Blüm, D. Gotta, K. Heitlinger, M. Schneider, J. Missimer, L. M. Simons, and K. Elsener, Phys. Rev. A **38**, 4395 (1988).
[23] L. M. Simons, D. Abbot, B. Bach, R. Bacher, A. Badertscher, P. Blüm, P. DeCecco, J. Eades, J. Egger, K. Elsener, D. Gotta, P. Hauser, K. Heitlinger, D. Horváth, F. Kottmann, E. Morenzoni, J. Missimer, J. J. Reidy, R. Siegel, D. Taqqu, and D. Viel, Nucl. Instrum. Methods Phys. Res. B **87**, 293 (1994).
[24] R. Bacher, P. Blüm, D. Gotta, K. Heitlinger, M. Schneider, J. Missimer, and L. M. Simons, Phys. Rev. A **39**, 1610 (1989).
[25] M. H. Prior, R. Marrus, and C. R. Vane, Phys. Rev. A **28**, 141 (1983).
[26] J. Missimer and L. M. Simons, Phys. Rep. **118**, 179 (1985).
[27] J. Missimer and L. M. Simons, Z. Phys. D **17**, 275 (1990).
[28] K. Kirch, D. Abbott, B. Bach, P. DeCecco, P. Hauser, D. Horváth, F. Kottmann, J. Missimer, R. T. Siegel, L. M. Simons, and D. Viel, Phys. Rev. Lett. **78**, 4363 (1997).
[29] G. W. F. Drake and L. L. Byer, Phys. Rev. A **32**, 713 (1985).
[30] B. Jeckelmann, P. F. A. Goudsmit, and H. J. Leisi, Phys. Lett. B **335**, 326 (1994).
[31] D. F. Anagnostopoulos *et al.*, PSI Proposal No. R-97-02.1, 1997.
[32] S. Lenz, G. Borchert, H. Gorke, D. Gotta, T. Siems, D. F. Anagnostopoulos, M. Augsburger, D. Chatellard, J.-P. Egger, D. Belmiloud, P. El-Khoury, P. Indelicato, M. Daum, P. Hauser, K. Kirch, and L. M. Simons, Phys. Lett. B **416**, 50 (1998).
[33] P. Hauser, K. Kirch, F. Kottmann, and L. M. Simons, Nucl. Instrum. Methods Phys. Res. A **411**, 389 (1998).
[34] D. Horváth, Czech. J. Phys., Sect. B **36**, 911 (1986).
[35] P. Ehrhart, F. J. Hartmann, E. Köhler, and H. Daniel, Z. Phys. A **311**, 259 (1983).
[36] O. Keski-Rahkonen and M. O. Krause, At. Data Nucl. Data Tables **14**, 139 (1974).
[37] P. Indelicato, O. Gorceix, and J. P. Desclaux, J. Phys. B **20**, 651 (1987).
[38] P. Indelicato and J. P. Desclaux, Phys. Rev. A **42**, 5139 (1990).
[39] J. P. Desclaux, in *Relativistic Multiconfiguration Dirac-Fock Package*, Methods and Techniques in Computational Chemistry, edited by E. Clementi (STEF, Cagliari, 1993), Vol. A.
[40] P. Indelicato, Phys. Rev. A **51**, 1132 (1995).
[41] J. E. Griffith, P. K. Haff, and T. A. Tombrello, Ann. Phys. (N.Y.) **87**, 1 (1974).
[42] H. Anderhub, H. Hofer, F. Kottmann, P. LeCoultre, D. Makowiecki, O. Pitzurra, B. Sapp, P. G. Seiler, M. Wälchli, D. Taqqu, P. Truttmann, A. Zehnder, and Ch. Tschalär, Phys. Lett. **71B**, 443 (1977).
[43] M. R. Harston, D. S. Armstrong, D. F. Measday, S. Stanislaus, P. Weber, and D. Horváth, Phys. Rev. A **44**, 103 (1991).
[44] V. I. Petrukhin, V. E. Risin, I. F. Samenkova, and V. M. Suvorov, Zh. Éksp. Teor. Fiz. **69**, 1883 (1975) [Sov. Phys. JETP **42**, 955 (1976)].
[45] V. I. Petrukhin and Yu. D. Prokoshkin, Dokl. Akad. Nauk SSSR **160**, 71 (1965) [Sov. Phys. Dokl. **10**, 33 (1965)].
[46] L. Schellenberg, P. Baeriswyl, R. Jacot-Guillarmod, B. Mischler, F. Mulhauser, C. Piller, and L. A. Schaller, in *Muonic Atoms and Molecules*, edited by L. A. Schaller and C. Petitjean (Birkhäuser Verlag, Basel, 1993), p. 187.
[47] D. Taqqu (private communication).
[48] G. Fottner, H. Daniel, P. Ehrhart, H. Hagn, F. J. Hartmann, E. Köhler, and W. Neumann, Z. Phys. A **304**, 333 (1982).